Detection of cytosolic *Shigella flexneri* via a C-terminal triple-arginine motif of GBP1 inhibits actin-based motility

Running title: GBP1 blocks actin-based motility

Anthony S. Piro[a], Dulcemaria Hernandez[a], Sarah Luoma[a], Eric. M. Feeley[a], Ryan Finethy[a], Azeb Yirga[a], Eva M. Frickel[b], Cammie F. Lesser[d,e] and Jörn Coers[a,f,#]

[a]Department of Molecular Genetics and Microbiology, Duke University Medical Center, Durham, NC 27710, USA; [b]The Francis Crick Institute, 1 Midland Road, London, NW1 1AT, UK; [d]Department of Medicine, Division of Infectious Diseases, Massachusetts General Hospital, Cambridge, MA 02139, USA; [e]Department of Microbiology and Immunobiology, Harvard Medical School, Boston, MA 02115, USA; [f]Department of Immunology, Duke University Medical Center, Durham, NC 27710, USA;

[#]corresponding author: E-mail: jorn.coers@duke.edu

Abstract

Dynamin-like guanylate binding proteins (GBPs) are gamma interferon (IFNγ)-inducible host defense proteins that can associate with cytosol-invading bacterial pathogens. Mouse GBPs promote the lytic destruction of targeted bacteria in the host cell cytosol but the antimicrobial function of human GBPs and the mechanism by which these proteins associate with cytosolic bacteria are poorly understood. Here, we demonstrate that human GBP1 is unique amongst the seven human GBP paralogs in its ability to associate with at least two cytosolic Gram-negative bacteria, *Burkholderia thailandensis* and *Shigella flexneri.* Rough lipopolysaccharide (LPS) mutants of *S. flexneri* co-localize with GBP1 less frequently than wildtype *S. flexneri*, suggesting that host recognition of O-antigen promotes GBP1 targeting to Gram-negative bacteria. The targeting of GBP1 to cytosolic bacteria, via a unique triple-arginine motif present in its C-terminus, promotes the co-recruitment of four additional GBP paralogs (GBP2, GBP3, GBP4 and GBP6). GBP1-decorated *Shigella* replicate but fail to form actin tails leading to their intracellular aggregation. Consequentially, wildtype but not the triple-arginine GBP1 mutant restricts *S. flexneri* cell-to-cell spread. Furthermore, human-adapted *S. flexneri,* through the action of one its secreted effectors, IpaH9.8, is more resistant to GBP1 targeting than the non-human-adapted bacillus *B. thailandensis*. These studies reveal that human GBP1 uniquely functions as an intracellular 'glue trap' inhibiting the cytosolic movement of normally actin-propelled Gram-negative bacteria. In response to this powerful human defense program *S. flexneri* has evolved an effective counter-defense to restrict GBP1 recruitment.

Importance

Several pathogenic bacterial species evolved to invade, reside and replicate inside the cytosol of their host cells. One adaptation common to most cytosolic bacterial pathogens is the ability to co-opt the host's actin polymerization machinery, in order to generate force for intracellular movement. This actin-based motility enables Gram-negative bacteria such as *Shigella* to propel themselves into neighboring cells thereby spreading from host cell to host cell without exiting the intracellular environment. Here, we show that the human protein GBP1 acts as a cytosolic 'glue trap' capturing cytosolic Gram-negative bacteria through a unique protein motif and preventing disseminated infections in cell culture models. To escape from this GBP1-mediated host defense, *Shigella* employs a virulence factor that prevents or dislodges the association of GBP1 with cytosolic bacteria. Thus, therapeutic strategies to restore GBP1 binding to *Shigella* may lead to novel treatment options for shigellosis in the future.

Introduction

Cell-autonomous immunity describes the ability of a single cell to defend itself against intracellular pathogens and constitutes an essential branch of the immune system (1, 2). Cell-autonomous immunity in vertebrates is often orchestrated by IFN-inducible genes (ISGs) (2). Amongst the most robustly expressed ISGs are those encoding dynamin-like guanylate binding proteins (GBPs) (3-5). GBPs control intrinsic antiviral, antiprotozoan and antibacterial immunity, are highly expressed in inflamed tissue, and can be predictive of infectious disease progressions (5-10). Since their discovery, seven human *GBP* orthologs and one pseudogene have been identified. The *GBP* genes are located within one gene cluster on chromosome 1 (11). Other vertebrate genomes contain comparable numbers of *GBP* orthologs: *e.g.* mice possess 11 genes in addition to 2 pseudogenes (12). Human and mouse GBPs share a high degree of homology with the most conserved region found within their N-terminal G domains. However, GBP protein family members are highly divergent from each other at their very C-terminal ends, both within and across different vertebrate species (11). The functional consequence of this C-terminal amino acid sequence variability has not been previously explored.

To exert many of their anti-microbial functions, GBPs specifically associate with intracellular microbes residing in the host cell cytosol or at pathogen-occupied supramolecular structures, which include viral replication complexes (10) and pathogen-containing vacuoles (3-5). Following pathogen recognition, GBPs are thought to deliver antimicrobial host factors to pathogen-containing vacuoles and to bacteria residing in the host cell cytosol, thereby enabling the execution of distinct defense pathways which include membranolytic destruction of cytosolic bacteria (13, 14), capture of microbes within degradative autolysosomes (7), and activation of inflammasomes (13-19). These studies clearly demonstrated the importance of GBPs in host defense against a broad spectrum of pathogens in a vertebrate host. However, because these previous studies were conducted almost exclusively in mouse models, it remains to be determined whether human GBPs execute functions comparable to their murine counterparts.

In this study we systematically tested all seven members of the human GBP protein family for their ability to co-localize with the cytosolic bacterial pathogens *Listeria monocytogenes, Shigella flexneri* and *Burkholderia thailandensis.* All of these bacterial species are equipped with the ability to co-opt the host actin polymerization machinery for actin-based cytosolic motility and cell-to-cell spread (20). While we failed to detect any co-localization between human GBPs and the Gram-positive bacterium, *L. monocytogenes,* we found that GBP1, independent of other human GBP paralogs, targeted both Gram-negative bacteria, *B. thailandensis* and *S. flexneri*. This specific interaction between GBP1 and bacteria, which is determined by a unique C-terminal triple-arginine motif, inhibits actin-tail formation of GBP1-decorated bacteria resulting in a reduction of bacterial cell-to-cell spread. We further observed that GBP1 targeted the non-human-adapted microbe *B. thailandensis* more efficiently than the human-adapted pathogen *S. flexneri* and identified the bacterial ubiquitin E3 ligase IpaH9.8 as a *S. flexneri* virulence factor that interferes with GBP1 recruitment to this professional cytosolic bacterium. Thus, this study provides a novel understanding of the role of human GBPs in immunity to bacterial pathogens and also defines a virulence strategy employed by a human-adapted microbe to escape from GBP1-regulated host defense.

Results

Human GBP1 co-localizes with cytosolic *S. flexneri* and *B. thailandensis*

Most known GBP-mediated antimicrobial functions require that GBPs directly localize to intracellular microbes or their surrounding vacuoles (3-5). Based on this premise we screened the entire set of human GBPs (GBP1 – 7) as ectopically expressed mCherry N-terminal fusion proteins in the human epithelial lung carcinoma cell line A549 for co-localization with the cytosolic bacterial pathogen *S. flexneri.* Expression of each fusion protein was detectable by Western blotting (Figure S1) and by immunofluorescence (Figure 1A). Unexpectedly, only a single member, GBP1, associated with cytosolic *S. flexneri,* as assessed at 1 and 3 hours post infection (hpi) in either naïve or IFNγ-primed A549 cells (Figure 1A). Association of GBP1 with individual *S. flexneri* bacteria was observed as early as 10 minutes post host cell invasion (data not shown and video S1). Similarly, we observed that GBP1 was the sole human GBP family member to co-localize with *B. thailandensis,* another cytosolic Gram-negative pathogen (Figure 1B). In contrast to the observed targeting of GBP1 to these Gram-negative bacteria, we failed to detect any co-localization with *L. monocytogenes,* a cytosolic Gram-positive pathogen (Figure 1C).

Targeting of GBP1 to *S. flexneri* is dependent on its functional G domain, CaaX box and a C-terminal triple-arginine motif

To determine which protein motifs and properties of GBP1 (Figure 2A) render it uniquely capable to detect cytosolic Gram-negative bacteria, we generated and screened a large set of GBP1 mutant variants for co-localization with cytosolic *S. flexneri*. Mutant variants previously established to be defective for GTP hydrolysis ($GBP1^{R48A}$) or nucleotide binding ($GBP1^{K51A}$ and $GBP1^{S52N}$) (21, 22) failed to associate with *S. flexneri* (Figure 2B). These findings were expected, because GTP binding and hydrolysis are required for GBP1 dimerization, protein polymerization and membrane binding (21-26). We also found that targeting to *S. flexneri* was dependent on the

C-terminal CaaX box of GBP1 (Figure 2B). This finding was also expected as CaaX box-dependent prenylation of GBP1 provides a lipid anchor critical for the membrane association of GBP1 (25-27).

Both GBP1 and GBP2 contain highly homologous N-terminal G domains and carry C-terminal CaaX boxes (11), yet only GBP1 efficiently associates with *S. flexneri* in A549 cells (Figure 1A). We therefore generated protein chimeras between GBP1 and GBP2 to map the motif that uniquely directs GBP1 to cytosolic bacteria. Most of the divergence between GBP1 and GBP2 sequences is found within the C-terminal subdomain (CTSD) consisting of α-helices α12 and α13, a short flexible region, and the CaaX box. We therefore swapped the CTSDs of GBP1 and GBP2 to generate two complementary chimeric proteins and found that the GBP1- but not GBP2-derived CTSD determined protein targeting to *S. flexneri* (Figure 2C). Swapping the CaaX boxes on the other hand only moderately reduced GBP1 targeting to bacteria (Figure 2C), indicating the existence of an additional motif within the GBP1-CTSD critical for bacterial recognition. Within the flexible region of CTSD we identified a GBP1-specific poly-basic protein motif (PBM), a 6 amino acid stretch containing 5 basic residues (KMRRRK). Deletion of these 6 residues or mutation of the triple-arginine cassette to triple-alanine abrogated co-localization of GBP1 with *S. flexneri* (Figure 2C). In a complementary approach, we found that insertion of the GBP1-PBM between GBP2 residues 586 and 587 ($GBP2^{+PBM}$) was sufficient to drive significant targeting of GBP2 to *S. flexneri* (Figure 2C). Swapping the GBP2 with the GBP1 CaaX box further improved the bacteria-targeting efficiency such that $GBP2^{+PBM+GBP1\text{-}CaaX}$ is recruited to *Shigella* at levels comparable to wildtype GBP1 (Figure 2D). These data demonstrate that a triple-arginine motif within the C-terminal PBM of GBP1 is essential and sufficient to equip both GBP1 and GBP2 with the ability to detect cytosolic *S. flexneri*, while the GBP1 CaaX box further improves targeting efficiency.

Triple-arginine motif controls delivery of GBP1 to sterilely damaged vacuoles.

To identify possible molecular targets for the C-terminal PBM of GBP1, we followed up on our previous published observation that GBP1 but none of its human paralogs detect sterilely damaged endogenous vacuoles in human embryonic kidney (HEK) 293T cells (28). The disruption of vacuoles leads to the cytosolic exposure of glycans that are normally confined to the vacuolar lumen. These exposed sugars then prompt the recruitment of the β-galactoside-binding lectin Galectin-3 as an established marker for loss of vacuolar integrity (29). To determine whether the PBM of GBP1 could promote the recognition of glycans, we tested its role in the delivery of GBP1 to ruptured vesicles. We first determined whether the structural requirements for the delivery of GBP1 to ruptured endosomes generally resembled those for the targeting of GBP1 to bacteria. In support of this premise, we observed that delivery of GBP1 to damaged endosomes was dependent on its functional G domain and CaaX box (Figure 3A). We further noticed that the CTSD of GBP1 was essential for the delivery of GBP1, and sufficient to promote recruitment of chimeric GBP2 protein, to damaged vesicles (Figure 3B). Deletion of PBM or mutation of the triple-arginine motif led to substantially reduced co-localization between Galectin-3-marked vacuoles and GBP1 (Figure 3B), indicating a functional role for the triple-arginine motif in the delivery of GBP1 to disrupted vesicles. These observations suggested that the triple-arginine motif of GBP1 directly or indirectly detects glycans.

S. flexneri mutants lacking O-antigen are targeted infrequently by GBP1

Because GBP1 detects broken vacuoles that are marked by cytosolically exposed polysaccharides normally confined to the vacuolar lumen, we speculated that bacterial surface-exposed polysaccharides could similarly underlie the recruitment of GBP1 to *S. flexneri.* We thus investigated whether GBP1 either directly or indirectly detects lipopolysaccharide (LPS), the main building block of Gram-negative bacterial envelope. Because O-antigen forms the outward sugar portion of LPS on the surface of bacteria, we tested GBP1 recruitment to the O-antigen-deficient

galU and *rfaL* 'rough' *S. flexneri* mutants, which enter the host cell cytosol of non-polarized epithelial cells at comparable frequencies (30). We found that co-localization of ectopically expressed (Figure 4C) or endogenous GBP1 (Figure 4C) to *S. flexneri* rough mutants was substantially diminished relative to GBP1 targeting to wildtype *S. flexneri,* indicating that O-antigen recognition plays an important role in GBP1 recognition of cytosolic Gram-negative bacteria.

We previously demonstrated that Galectin-3 interacts with a subset of murine GBPs and promotes their recruitment to *Legionella*- as well as *Yersinia*-containing vacuoles (28). Because Galectin-3 binds to O-antigen as well as the inner core of LPS (31), we hypothesized that Galectin-3 could promote the delivery of GBP1 to the Gram-negative bacterium *S. flexneri.* However, we observed that ectopically expressed GBP1 co-localized with *S. flexneri* with comparable frequencies in wildtype and Galectin-3 deficient mouse embryonic fibroblasts (MEFs) (Figure S2). Together, these data suggest GBP1 detects cytosolic *S. flexneri* in an O-antigen-dependent but Galectin-3-independent manner.

GBP1-decorated *S. flexneri* replicate within intracellular bacterial clusters

Previous work demonstrated the lytic destruction of GBP-bound cytosolic bacteria in mouse cells (13, 14). To assess whether recruitment of human GBP1 to *S. flexneri* would similarly drive bactericidal effects, we used an IPTG-inducible GFP reporter system as a bacterial viability indicator. In these experiments, we infected HeLa cells with reporter-positive *S. flexneri,* then induced GFP expression with IPTG at 2 hpi and stained cells for endogenous GBP1 and LPS at 4 hpi (Figure 5A). As expected, inhibition of bacterial translation with chloramphenicol treatment at 2 hpi blocked detectable GFP expression at 4hpi (Figure 5B), thus validating the reporter system. In the absence of chloramphenicol, GBP1-targeted and -untargeted bacteria were GFP-positive at comparable frequencies, indicating that GBP1 recruitment to *S. flexneri* fails to promote bacterial killing at this time point (Figure 5B). Instead, we noticed that GBP1-positive bacteria form

intracellular clusters. To determine whether GBP1 could be responsible for this clustering effect, we generated HeLa cells that lack *GBP1* (*GBP1*^{KO}) (Figure 5C). Following IFNγ priming to induce expression of GBPs, we observed reduced bacterial clustering in two independent *GBP1*^{KO} clonal cell lines as compared to the parental HeLa cells (Figure 5D). Bacterial clustering was restored in *GBP1*^{KO} cells by ectopically expressing wildtype GBP1 but not a triple-arginine mutant (Figure 5D). Furthermore, we found that GBP1-decorated, clustered bacteria not only remained viable but continued to divide (Figure 5E and video S2). Thus, our observations indicate that triple-arginine-dependent delivery of GBP1 to cytosolic *S. flexneri* promotes bacterial clustering but fails to execute bactericidal or bacteriostatic activities.

GBP1 inhibits actin-based motility in a triple-arginine motif-dependent manner

GBP1-decorated *S. flexneri* cluster intracellularly and therefore phenocopy *S. flexneri* Δ*icsA* mutants (Figure 6A) that lack the ability to form actin tails and hence are non-motile inside the host cell cytosol (32). Thus, we hypothesized that GBP1 blocks *S. flexneri* actin tail formation. In support of this hypothesis we observed a marked reduction in actin tails associated with GBP1-tagged versus -untagged *S. flexneri* in 293T cells expressing mCherry-GBP1 (Figure 6A). To complement these GBP1 overexpression studies, we scored actin tail-positive bacteria in wildtype versus *GBP1*^{KO} HeLa cells. We found that IFNγ priming reduced the number of bacteria with actin tails in wildtype but not in *GBP1*^{KO} cells (Figure 6B). Complementation of *GBP1*^{KO} cells with wildtype GBP1 but not the triple-arginine mutant (GBP1$^{R584\text{-}586A}$) dramatically reduced the number of actin tail-positive bacteria to levels observed in IFNγ-primed wildtype cells (Figure 6B). As expected, GBP1-mediated inhibition of actin tail formation correlated with a GBP1-mediated block in cell-to-cell spread (Figure 6C). Inhibition of cell-to-cell spread was restored in *GBP1*^{KO} cells complemented with wildtype but not the triple-arginine mutant (GBP1$^{R584\text{-}586A}$) (Figure 6D), indicating that GBP1 targeting to bacteria is required for inhibition of bacterial cell-to-cell spread.

Endogenous GBP1 associates with *S. flexneri* and recruits additional GBP paralogs in HeLa but not in A549 cells

GBP1 frequently forms heterodimers with other members of the GBP family such as GBP2 (3-5). To determine whether GBP1 recruits other GBP paralogs to cytosolic *S. flexneri,* we ectopically expressed mCherry-tagged human GBP1-7 in wildtype and *GBP1*^{KO} HeLa cells and monitored for subcellular localization of each with cytosolic *S. flexneri*. We found that ectopically expressed GBP2, and to a lesser extent GBP3, GBP4 and GBP6 co-localized with *S. flexneri* in HeLa cells in a GBP1-dependent manner (Figure 7A). This finding was curious, as we had not observed any co-localization of these GBP paralogs with *S. flexneri* in wildtype A549 cells (Figure 1A). We therefore monitored the subcellular localization of endogenous GBP1 in A549 cells and found that endogenous GBP1 targeted *S. flexneri* in HeLa but not in A549 cells (Figure 7B), which correlated with reduced expression of GBP1 protein in A549 compared to HeLa cells (Figure 7C). While endogenous GBP1 failed to decorate *S. flexneri* in A549 cells, we noticed that in the same cell line about 40% of cytosolic *B. thailandensis* stained positive for endogenous GBP1 (Figure 7B). These data suggested that *B. thailandensis* is more susceptible to GBP1 targeting than *S. flexneri.* To test this hypothesis, we generated a titratable, *i.e.* anhydrotetracycline (aTc)-inducible expression system for GBP1 (Figure 7D). As expected, higher GBP1 expression levels promoted more frequent co-localization with either bacterium. However, the overall frequency of GBP1 co-localization was significantly higher for *B. thailandensis* than for *S. flexneri* (Figure 7E). These data indicated that *S. flexneri* is more resistant to GBP1 targeting than *B. thailandensis* and therefore suggested that *S. flexneri* actively interferes with cytosolic detection by GBP1.

IpaH9.8 blocks GBP1 recruitment and GBP1-mediated inhibition of actin-based motility

To account for our observations, we hypothesized that an effector secreted by the *Shigella* type 3 secretion system (T3SS) interferes with GBP1 targeting to cytosolic bacteria. To test this hypothesis, we monitored co-localization of GBP1 with two *S. flexneri* mutants deficient for the secretion of distinct subsets of type III effectors. A bacterial mutant lacking Spa15, the chaperone required for the secretion of the effectors IpaA, IpgB1, IpgB2, OspB, OspC1, OspC2, OspC3, OspD1 and OspD2 (33-36), was targeted with the same efficiency as wildtype *S. flexneri* (Figure 8A). However, Δ*mxiE Shigella,* a strain lacking the transcription factor that controls expression of second phase *S. flexneri* effectors including all IpaH effectors as well as OspB, OspC1, OspE1, OspE2, OspF, OspG and VirA (37-39), co-localized more frequently with GBP1 than wildtype *S. flexneri* in both A549 and HeLa cells (Figure 8A). These findings indicated that one or more mxiE-dependent T3SS effectors interfered with GBP1 function. To identify this virulence factor, we screened *S. flexneri* mutants deficient in individual mxiE-dependent T3SS effectors encoded on the *S. flexneri* virulence plasmid and found that Δ*ipaH9.8* mimicked the Δ*mxiE* phenotype (Figure 8B). Further, we found that Δ*ipaH9.8* was deficient for cell-to-cell spread in parental HeLa but not in *GBP1*^{KO} cells (Figure 8C), indicating that IpaH9.8-mediated interference with GBP1 targeting is critical for *S. flexneri* dissemination throughout the colonic epithelium. Cell-to-cell spread of the Δ*mxiE* mutant compared to wildtype *S. flexneri* was still moderately diminished in *GBP1*^{KO} cells, suggesting that one or more additional mxiE-controlled effectors other than ipaH9.8 promote cellular dissemination (Figure 8C).

Discussion

Many cell-autonomous defense mechanisms depend on the ability of the host cell to detect the precise location of an intracellular microbe inside an infected host cell (40). Pathogen-containing vacuoles are targeted by GBPs following immune recognition through missing-self or aberrant-self mechanisms (28, 41, 42), but the mechanism by which GBPs detect cytosolic pathogens had not previously been investigated. Here, we demonstrate that human GBP1 contains a unique triple-arginine motif within its flexible C-terminal region, which mediates the delivery of GBP1 to the Gram-negative cytosolic pathogen *S. flexneri.* We also demonstrate in this study that *S. flexneri* rough mutants lacking LPS O-antigen are targeted less efficiently by GBP1 than the co-isogenic wildtype strain. These observations suggest that the triple-arginine motif of human GBP1 either directly or indirectly interacts with the polysaccharide portion of LPS on the bacterial surface.

GBP1 binding to bacteria still occurs in the absence of O-antigen, albeit less efficiently. One possible explanation for this observation is that GBP1 associates with LPS through two or more distinct interactions, as has been described for Galectin-3. Galectin-3 binds to LPS through a high-affinity interaction with O-antigen as well as a low-affinity interaction with the inner LPS core (31). Alternatively, GBP1 could be recruited to bacteria through an additional LPS-independent mechanism. Future *in vitro* binding studies are required to test whether GBP1 binds to Gram-negative bacteria directly or indirectly, and to identify the specific binding substrate(s) or interaction partner(s) of the C-terminal triple-arginine motif essential for immune targeting of cytosolic *S. flexneri* by GBP1.

Previous work demonstrated that deposition of murine GBP2 on the cytosolic bacterial pathogen *Francisella novicida* results in bacteriolysis (13, 14). Similarly, murine GBPs also promote the lytic destruction of *S. flexneri* (43). Unexpectedly, we found that the delivery of human GBP1 to cytosolic *S. flexneri* is insufficient to kill bacteria or halt their replication. Instead, we

observed that GBP1-bound bacteria fail to form actin tails and are consequentially restricted for efficient cell-to-cell spread. These observations were confirmed by an independent report published during the preparation of our manuscript (44). The differences between mouse and human in regards to the consequences of GBP targeting are intriguing and warrant future investigations to determine, for instance, whether the lytic pathway present in mouse cells is absent from human cells. The latter model is supported by a report demonstrating that GBP-dependent recruitment of the IFN-inducible GTPases Irgb10 to cytosolic *F. novicida* is required for bacteriolysis in mouse cells (45). Importantly, genes encoding Irgb10 and its paralogous subset of immunity related GTPases (IRGs) with a canonical GxxxxGKS P-loop sequence are absent from the human genome (46, 47), potentially accounting for the absence of an intracellular bacteriolytic pathway in human cells.

The dysregulation of cell-autonomous defense programs by *S. flexneri* is paramount to the microbes' ability to colonize its human host and establish an infection (48). In agreement with two studies published during the preparation of our manuscript (43, 44), we found that the translocated bacterial ubiquitin E3 ligase IpaH9.8 inhibits the association of GBP1 with cytosolic *S. flexneri* in human cells. We did not investigate the mechanism by which IpaH9.8 interferes with GBP1 localization to bacteria, but the aforementioned studies demonstrated that IpaH9.8 ubiquitinates GBP1 and promotes its degradation via the proteasome (43, 44). While proteolytic degradation was clearly demonstrated at infections with high multiplicity of infection (MOI) or in cells ectopically expressing IpaH9.8 (43, 44), we failed to observe a pronounced decrease in GBP1 protein expression in cells infected with *S.flexneri* under the infection conditions used in our studies (Figure 7C). Furthermore, video microscopy data suggest that GBP1 ubiquitination by IpaH9.8 helps to dislodge GBP1 from targeted bacteria (44). We therefore propose that ubiquitination by IpaH9.8 not only tags GBP1 for proteolytic degradation but also directly blocks binding of GBP1 to bacteria and/or removes GBP1 from already targeted bacteria. Importantly, Li et al. demonstrated

that IpaH9.8 promotes poly-ubiquitination of the GBP1 residues K582 and K587 (43), which flank the triple-arginine motif essential for recruiting GBP1 to *S. flexneri.* Whether PBM ubiquitination blocks GBP1 binding to bacteria through steric hindrance will be investigated in future studies.

Materials and Methods

Cell Lines and Culture

Primary WT and *Galectin-3*^{KO} (49) MEFs were made from C57BL/6J background mice acquired from the Jackson Laboratory. MEFs, A549, 293T, and HeLa cells were maintained at 37° and 5% CO_2 in DMEM supplemented with 10% heat inactivated fetal bovine serum, nonessential amino acids (Gibco), and 55 μM β-mercaptoethanol. *GBP1*^{KO} lines were derived from HeLa-Cas9 cells, which contains a stably integrated Cas9 expression vector, lentiCas9-Blast (50). HeLa-Cas9 cells were transiently transfected with two guide RNAs directed against exon 6, GBP1-2 (TTGATCGGCCCGTTCACCGC) and GBP1-3 (TCCGGATACAGAGTCTGGGC), to introduce a predicted 64 bp deletion. Single clones were isolated by dilution. Resulting alleles are described in Table S1. All instances of IFNγ priming were done overnight at 200 U/ml.

Bacterial Strains and Infections

Bacterial strains are summarized in Table S2. 2457T *S.flexneri*-derived Δ*mxiE,* Δ*ospB,* Δ*ospC1,* Δ*virA,* Δ*IpaH1.4,* Δ*IpaH4.5,* Δ*IpaH7.8* and Δ*IpaH9.8* were constructed using the λ red recombinase-mediated recombination system (51) using DNA oligomers listed in Table S3. GFP$^+$ *S.flexneri* stains contain the vector pGFPmut2 (52). The IPTG-inducible GFP vector pRK2-IPTG-GFP was a gift from Wendy Picking. *S.flexneri* was grown at 37° on tryptic soy agar plates containing 0.01% Congo Red, as well as 50 μg/ml carbenicillin for pGFPmut2 and PRK2-IPTG-GFP containing strains. For infections, 5 ml tryptic soy broth (TSB) was inoculated with a single Congo red-positive colony and grown overnight at 37° with shaking. Saturated cultures were diluted 1:50 in 5 ml fresh TSB and incubated for 2.5-3 h at 37° with shaking. Bacteria were diluted in pre-warmed cell culture medium, and spun onto cells for 10 minutes at 700 x g. Plates were incubated at 37° for 30 minutes, then washed twice with Hanks Balanced Salt Solution (HBSS), followed by addition of cell

culture medium containing 25 μg/ml gentamicin and further incubation at 37°. Unless otherwise specified, cells were infected at an MOI of 50. For time lapse microscopy and plaque assays, $5x10^7$ bacteria were harvested by centrifugation and incubated in 1 ml phosphate buffered saline (PBS) containing 5 μg/ml poly-D-lysine at 37° for 15 minutes with shaking, as described (53). Poly-D-lysine pre-treated bacteria were then used for infection, as above. *B. thailandensis* wiltype strain E264 carrying a GFP-expression construct was a gift from Edward Miao. *B.thailandensis* +GFP was grown at 37° on LB plates containing 100 ug/ml trimethoprim. For infections, overnight cultures were diluted 1:20 in LB + trimethoprim and grown for 3 h at 37° with shaking. Cells were infected at an MOI of 100, as above. Infected plates were incubated at 37° for 2.5 h, washed twice with HBSS, and incubated in the presence of 30 μg/ml kanamycin for 2 h. Kanamycin containing medium was then replaced with medium without antibiotics, and plates were incubated at 37° to 8 hpi. GFP^+ wildtype *L. monocytogenes* strain 10403S was previously described (54) and grown at 37° on brain heart infusion (BHI) plates containing 10 μg/ml streptomycin and 7.5 μg/ml chloramphenicol. Infections were carried out in an identical manner to *S.flexneri* using saturated overnight cultures grown at 37° with shaking. Cells were infected with *L. monocytogenes* at an MOI of 5.

Design of GBP Expression Constructs

Vectors containing mCherry-tagged constructs are derivatives of pmCherry-C1 (Clontech), and were constructed using DNA oligomers and restriction endonucleases listed in Table S4. For the chimeric constructs, $GBP1/2^{CTSD}$ and $GBP2/1^{CTSD}$, two synonymous mutations were introduced into GBP1 codons 478 and 479 of pmCherry-GBP1 using Quickchange site directed mutagenesis with GBP1-BclI oligomers (Table S5). These mutations introduced a BclI restriction endonuclease site within the sequence encoding the flexible region between helices 11 and 12. Following propagation of pmCherry-$GBP1^{BclI}$ and pmCherry-GBP2 in *dam*$^-$/*dcm*$^-$ *E.coli* (New England

Biolabs), BclI digestion and T4 Ligase-dependent repair was used to exchange the fragment encoding the C-terminal regions of the two proteins. All other mCherry-tagged chimeric and mutant constructs were constructed using Quickchange site directed mutagenesis with the primers listed in Table S5. GBP2$^{+PBM+GBP1\text{-}CaaX}$ was constructed stepwise from pmCherry-GBP2^{+PBM} mutated with GBP2/1^{CaaX}- and then GBP2^{I587A}-oligomers. Tetracycline-inducible GBP1 was constructed by inserted the *GBP1* ORF into the third generation Tet-On vector, pInducer20 (55), using Gateway Cloning Technology with GBP1-attB oligomers listed in Table S5. GBP1$^{R584\text{-}586A}$ was constructed by mutating the entry vector, pDONR221-GBP1, via Quickchange SDM using GBP1$^{R584\text{-}586A}$-oligomers prior to Gateway LR reactions.

Immunofluorescence Microscopy, actin tail analysis, Time-Lapse Microscopy and CPP assays

For standard microscopy cells were fixed in 4% paraformaldehyde and permeabilized with 0.25% Triton X-100 in PBS. Coverslips were probed with a 1:150 dilution of a rabbit monocolonal antibody against human GBP1 (Abcam ab131255) and/or a 1:50 dilution of a mouse monoclonal antibody against LPS (Raybiotech DS-MB-01267), followed by AlexaFluor conjugated secondary antibodies and 4 µg/ml of the nuclear dye Hoechst, where appropriate. For actin tail analysis, 1:40 Phalloidin conjugated to AlexFluor488 was added to the secondary antibody mix. For each field of view, Z-stacks were taken at 0.5 µm intervals on a Zeiss 710 inverted confocal to encompass the thickness of the cells. The percentage of bacteria with tails was determined by referencing across the collected Z-stacks through blinded analysis. For time-lapse microscopy *GBP1^{KO}* HeLa cells were plated in 35 mm glass bottom plates (MatTek) and transfected with pmCherry-GBP1. Cells were infected with GFP^{+} *S.flexneri* pre-treated with poly-D-lysine at an MOI of 10. Cells were imaged in DMEM without phenol red containing 5% FBS and 25 µg/ml gentamicin. Calcium phosphate precipitate (CPP) assays were carried out in 293T cells stably expressing YFP-Galectin-3 and

transiently transfected with mCherry-tagged GBP constructs, as described in(28). Calcium phosphate precipitate (CPP) assays were carried out in 293T cells stably expressing YFP-Galectin-3 and transiently transfected with mCherry-tagged GBP constructs, as described in(28).

IPTG-Inducible GFP Viability Assay

HeLa cells were stimulated overnight with 200 U/ml IFNγ and infected with *S.flexneri* containing the IPTG-inducible GFP vector, pRK2-IPTG-GFP. At 2 hpi, IPTG was added to a concentration of 1mM. Chloramphenicol was also added to a concentration of 60 µg/ml for negative controls. Coverslips were incubated for an additional 2 h before being fixed and stained with anti-LPS and anti-GBP1 antibodies, as described above.

***S.flexneri* Cluster Analysis**

Images were thresholded to remove background signal, and were subjected to connexity analysis to identify adjacent structures using the 3D objects counter in FIJI. Briefly, this process takes a pixel of interest and assesses whether the 26 surrounding pixels, (8 in plane, 9 above and below), contain signal above threshold. All adjacent pixels above threshold are then considered to be part of the same object. Each object is assigned a unique tag. The image is then subjected to a second pass to correctly identify connected items in three-dimensional space. The volume of each object is calculated and bacterial cluster analyzed. A volume representing individual and dividing bacteria was determined, and a threshold above this value was used to identify clusters.

Plaque Assays

Plaque assays were performed essentially as previously described (56). Cells were plated to confluence in 35 mm glass bottom plates and stimulated overnight with 200 U/ml IFNγ. Cells were infected at an MOI of $5x10^{-4}$ with GFP^{+} *S.flexneri* pre-treated with poly-D-lysine. Following 30

minutes of infection at 37°, plates were washed twice with HBSS and overlaid with 1.5 ml DMEM without phenol red supplemented with 5% FBS and containing 25 ug/ml gentamicin, 200 U/ml IFNγ, 50 ug/ml carbenicillin, and 0.5% agarose. Plates were incubated for 10 minutes at room temperature before addition of 1 ml of cell culture medium without agarose. Plaques were visualized using phase contrast and fluorescence microscopy at 24 hpi, and the Feret diameter of individual plaques was determined using FIJI. For plaque assays using *GBP1*^{KO} cells complemented with pInducer-GBP1 or -GBP1$^{R584-586}$, cells were stimulated overnight with 1 µg/ml aTc.

Titration of GBP1 Expression from Tet-Inducible Expression System and Immunoblots

GBP1^{KO} cells stably transduced with pInducer-GBP1 constructs were incubated overnight with cell culture medium containing the indicated concentrations of aTc. Cells were lysed in RIPA buffer containing 1X protease inhibitor cocktail (Sigma) for 5 minutes on ice. Lysates were spun for 10 minutes at maximum speed in a microcentrifuge at 4° C, then combined with an equivalent volume of 2X Laemmli Sample Buffer containing β-mercaptoethanol, and incubated at 95° for 10 minutes. Samples were run on 4-15% Mini-PROTEAN TGX gels (Bio Rad) and transferred to nitrocellulose. Immunoblots were probed with 1:1,000 anti-GBP1 (Abcam ab131255), 1:1,000 anti-mCherry rabbit polyclonal (Abcam ab183628), or anti-GAPDH rabbit polyclonal (Abcam ab9485), followed by horseradish peroxidase-conjugated anti-rabbit IgG (Invitrogen).

Statistical Analyses. Data analysis was performed using GraphPad Prism 6.0 software. Data shown are mean ± standard error of the mean (SEM) unless otherwise indicated. Statistical significance was calculated using 1-way or 2-way ANOVA or student t-test, as indicated. Significance was defined as (****$P < 0.0001$; ***$P < 0.001$; **$P < 0.01$; *$P < 0.05$).

Author contribution

Conceptualization: A.S.P. and J.C.; Methodology: A.S.P. and J.C.; Investigation: A.S.P., D.H., S.L., E.M.F., R.S., S.W.; Writing– Original Draft: J.C.; Writing – Review & Editing: A.S.P. and J.C.; Funding Acquisition: C.F.L. and J.C.; Resources: E-M.F., C.F.L.; Supervision: J.C.

Funding information

This work was supported by National Institute Health grants AI103197 (to JC) and AI064285 to (CFL). JC holds an Investigator in the Pathogenesis of Infectious Disease Awards from the Burroughs Wellcome Fund and CFL is the MGH d'Arbeloff research scholar.

Acknowledgement

We thank Edward Miao from UNC Chapel Hill for sharing *B. thailandensis* strains, Marcia Goldberg from Harvard Medical School for providing the Δ*iscA S. flexneri* mutant and co-isogenic wildtype strains, Anthony Maurelli from the University of Florida for providing the *S. flexneri galU* and *rfaL* mutant and co-isogenic wildtype strains and Wendy Picking for providing pRK2-IPTG-GFP. We thank So Young Kim from the Duke Functional Genomics core for the production of HeLa *GBP1*^{KO} cells. We thank members of the Coers and Tobin labs for helpful discussions.

References

1. **Howard JC.** 2007. Introduction: cell-autonomous immunity. Microbes Infect **9:**1633-1635.
2. **MacMicking JD.** 2012. Interferon-inducible effector mechanisms in cell-autonomous immunity. Nat Rev Immunol **12:**367-382.
3. **Kim BH, Chee JD, Bradfield CJ, Park ES, Kumar P, MacMicking JD.** 2016. Interferon-induced guanylate-binding proteins in inflammasome activation and host defense. Nat Immunol **17:**481-489.
4. **Man SM, Place DE, Kuriakose T, Kanneganti TD.** 2017. Interferon-inducible guanylate-binding proteins at the interface of cell-autonomous immunity and inflammasome activation. J Leukoc Biol **101:**143-150.
5. **Pilla-Moffett D, Barber MF, Taylor GA, Coers J.** 2016. Interferon-inducible GTPases in host resistance, inflammation and disease. J Mol Biol doi:10.1016/j.jmb.2016.04.032.
6. **Deshiere A, Joly-Beauparlant C, Breton Y, Ouellet M, Raymond F, Lodge R, Barat C, Roy MA, Corbeil J, Tremblay MJ.** 2017. Global Mapping of the Macrophage-HIV-1 Transcriptome Reveals that Productive Infection Induces Remodeling of Host Cell DNA and Chromatin. Sci Rep **7:**5238.
7. **Kim BH, Shenoy AR, Kumar P, Das R, Tiwari S, MacMicking JD.** 2011. A family of IFN-gamma-inducible 65-kD GTPases protects against bacterial infection. Science **332:**717-721.
8. **Krapp C, Hotter D, Gawanbacht A, McLaren PJ, Kluge SF, Sturzel CM, Mack K, Reith E, Engelhart S, Ciuffi A, Hornung V, Sauter D, Telenti A, Kirchhoff F.** 2016. Guanylate Binding Protein (GBP) 5 Is an Interferon-Inducible Inhibitor of HIV-1 Infectivity. Cell Host Microbe **19:**504-514.
9. **Zak DE, Penn-Nicholson A, Scriba TJ, Thompson E, Suliman S, Amon LM, Mahomed H, Erasmus M, Whatney W, Hussey GD, Abrahams D, Kafaar F, Hawkridge T, Verver S, Hughes EJ, Ota M, Sutherland J, Howe R, Dockrell HM, Boom WH, Thiel B, Ottenhoff TH, Mayanja-Kizza H, Crampin AC, Downing K, Hatherill M, Valvo J, Shankar S, Parida SK, Kaufmann SH, Walzl G, Aderem A, Hanekom WA, Acs, groups GCcs.** 2016. A blood RNA signature for tuberculosis disease risk: a prospective cohort study. Lancet **387:**2312-2322.
10. **Biering SB, Choi J, Halstrom RA, Brown HM, Beatty WL, Lee S, McCune BT, Dominici E, Williams LE, Orchard RC, Wilen CB, Yamamoto M, Coers J, Taylor GA, Hwang S.** 2017. Viral Replication Complexes Are Targeted by LC3-Guided Interferon-Inducible GTPases. Cell Host Microbe **22:**74-85 e77.
11. **Olszewski MA, Gray J, Vestal DJ.** 2006. In silico genomic analysis of the human and murine guanylate-binding protein (GBP) gene clusters. J Interferon Cytokine Res **26:**328-352.
12. **Li G, Zhang J, Sun Y, Wang H, Wang Y.** 2009. The evolutionarily dynamic IFN-inducible GTPase proteins play conserved immune functions in vertebrates and cephalochordates. Mol Biol Evol **26:**1619-1630.
13. **Man SM, Karki R, Malireddi RK, Neale G, Vogel P, Yamamoto M, Lamkanfi M, Kanneganti TD.** 2015. The transcription factor IRF1 and guanylate-binding proteins target activation of the AIM2 inflammasome by Francisella infection. Nat Immunol doi:10.1038/ni.3118.
14. **Meunier E, Wallet P, Dreier RF, Costanzo S, Anton L, Ruhl S, Dussurgey S, Dick MS, Kistner A, Rigard M, Degrandi D, Pfeffer K, Yamamoto M, Henry T, Broz P.** 2015. Guanylate-binding proteins promote activation of the AIM2 inflammasome during infection with Francisella novicida. Nat Immunol doi:10.1038/ni.3119.
15. **Meunier E, Dick MS, Dreier RF, Schurmann N, Kenzelmann Broz D, Warming S, Roose-Girma M, Bumann D, Kayagaki N, Takeda K, Yamamoto M, Broz P.** 2014. Caspase-11 activation requires lysis of pathogen-containing vacuoles by IFN-induced GTPases. Nature **509:**366-370.
16. **Shenoy AR, Wellington DA, Kumar P, Kassa H, Booth CJ, Cresswell P, MacMicking JD.** 2012. GBP5 promotes NLRP3 inflammasome assembly and immunity in mammals. Science **336:**481-485.
17. **Finethy R, Jorgensen I, Haldar AK, de Zoete MR, Strowig T, Flavell RA, Yamamoto M, Nagarajan UM, Miao EA, Coers J.** 2015. Guanylate Binding Proteins enable rapid activation of canonical and noncanonical inflammasomes in Chlamydia-infected macrophages. Infect Immun doi:10.1128/IAI.00856-15.
18. **Pilla DM, Hagar JA, Haldar AK, Mason AK, Degrandi D, Pfeffer K, Ernst RK, Yamamoto M, Miao EA, Coers J.** 2014. Guanylate binding proteins promote caspase-11-dependent pyroptosis in response to cytoplasmic LPS. Proc Natl Acad Sci U S A **111:**6046-6051.
19. **Finethy R, Luoma S, Orench-Rivera N, Feeley EM, Haldar AK, Yamamoto M, Kanneganti TD, Kuehn MJ, Coers J.** 2017. Inflammasome Activation by Bacterial Outer Membrane Vesicles Requires Guanylate Binding Proteins. MBio **8**.

20. **Lamason RL, Welch MD.** 2017. Actin-based motility and cell-to-cell spread of bacterial pathogens. Curr Opin Microbiol **35:**48-57.
21. **Praefcke GJ, Geyer M, Schwemmle M, Robert Kalbitzer H, Herrmann C.** 1999. Nucleotide-binding characteristics of human guanylate-binding protein 1 (hGBP1) and identification of the third GTP-binding motif. J Mol Biol **292:**321-332.
22. **Praefcke GJ, Kloep S, Benscheid U, Lilie H, Prakash B, Herrmann C.** 2004. Identification of residues in the human guanylate-binding protein 1 critical for nucleotide binding and cooperative GTP hydrolysis. J Mol Biol **344:**257-269.
23. **Prakash B, Praefcke GJ, Renault L, Wittinghofer A, Herrmann C.** 2000. Structure of human guanylate-binding protein 1 representing a unique class of GTP-binding proteins. Nature **403:**567-571.
24. **Prakash B, Renault L, Praefcke GJ, Herrmann C, Wittinghofer A.** 2000. Triphosphate structure of guanylate-binding protein 1 and implications for nucleotide binding and GTPase mechanism. EMBO J **19:**4555-4564.
25. **Britzen-Laurent N, Bauer M, Berton V, Fischer N, Syguda A, Reipschlager S, Naschberger E, Herrmann C, Sturzl M.** 2010. Intracellular trafficking of guanylate-binding proteins is regulated by heterodimerization in a hierarchical manner. PLoS One **5:**e14246.
26. **Shydlovskyi S, Zienert AY, Ince S, Dovengerds C, Hohendahl A, Dargazanli JM, Blum A, Gunther SD, Kladt N, Sturzl M, Schauss AC, Kutsch M, Roux A, Praefcke GJK, Herrmann C.** 2017. Nucleotide-dependent farnesyl switch orchestrates polymerization and membrane binding of human guanylate-binding protein 1. Proc Natl Acad Sci U S A **114:**E5559-E5568.
27. **Modiano N, Lu YE, Cresswell P.** 2005. Golgi targeting of human guanylate-binding protein-1 requires nucleotide binding, isoprenylation, and an IFN-gamma-inducible cofactor. Proc Natl Acad Sci U S A **102:**8680-8685.
28. **Feeley EM, Pilla-Moffett DM, Zwack EE, Piro AS, Finethy R, Kolb JP, Martinez J, Brodsky IE, Coers J.** 2017. Galectin-3 directs antimicrobial guanylate binding proteins to vacuoles furnished with bacterial secretion systems. Proc Natl Acad Sci U S A **114:**E1698-E1706.
29. **Coers J.** 2017. Sweet host revenge: Galectins and GBPs join forces at broken membranes. Cell Microbiol doi:10.1111/cmi.12793.
30. **Kohler H, Rodrigues SP, McCormick BA.** 2002. Shigella flexneri Interactions with the Basolateral Membrane Domain of Polarized Model Intestinal Epithelium: Role of Lipopolysaccharide in Cell Invasion and in Activation of the Mitogen-Activated Protein Kinase ERK. Infect Immun **70:**1150-1158.
31. **Mey A, Leffler H, Hmama Z, Normier G, Revillard JP.** 1996. The animal lectin galectin-3 interacts with bacterial lipopolysaccharides via two independent sites. J Immunol **156:**1572-1577.
32. **Bernardini ML, Mounier J, d'Hauteville H, Coquis-Rondon M, Sansonetti PJ.** 1989. Identification of icsA, a plasmid locus of Shigella flexneri that governs bacterial intra- and intercellular spread through interaction with F-actin. Proc Natl Acad Sci U S A **86:**3867-3871.
33. **Page AL, Sansonetti P, Parsot C.** 2002. Spa15 of Shigella flexneri, a third type of chaperone in the type III secretion pathway. Mol Microbiol **43:**1533-1542.
34. **Parsot C, Ageron E, Penno C, Mavris M, Jamoussi K, d'Hauteville H, Sansonetti P, Demers B.** 2005. A secreted anti-activator, OspD1, and its chaperone, Spa15, are involved in the control of transcription by the type III secretion apparatus activity in Shigella flexneri. Mol Microbiol **56:**1627-1635.
35. **Costa SC, Lesser CF.** 2014. A multifunctional region of the Shigella type 3 effector IpgB1 is important for secretion from bacteria and membrane targeting in eukaryotic cells. PLoS One **9:**e93461.
36. **Hachani A, Biskri L, Rossi G, Marty A, Menard R, Sansonetti P, Parsot C, Van Nhieu GT, Bernardini ML, Allaoui A.** 2008. IpgB1 and IpgB2, two homologous effectors secreted via the Mxi-Spa type III secretion apparatus, cooperate to mediate polarized cell invasion and inflammatory potential of Shigella flexenri. Microbes Infect **10:**260-268.
37. **Ashida H, Toyotome T, Nagai T, Sasakawa C.** 2007. Shigella chromosomal IpaH proteins are secreted via the type III secretion system and act as effectors. Mol Microbiol **63:**680-693.
38. **Kane CD, Schuch R, Day WA, Jr., Maurelli AT.** 2002. MxiE regulates intracellular expression of factors secreted by the Shigella flexneri 2a type III secretion system. J Bacteriol **184:**4409-4419.

39. **Mavris M, Sansonetti PJ, Parsot C.** 2002. Identification of the cis-acting site involved in activation of promoters regulated by activity of the type III secretion apparatus in Shigella flexneri. J Bacteriol **184:**6751-6759.
40. **Coers J.** 2013. Self and Non-self Discrimination of Intracellular Membranes by the Innate Immune System. PLoS Pathog **9:**e1003538.
41. **Haldar AK, Saka HA, Piro AS, Dunn JD, Henry SC, Taylor GA, Frickel EM, Valdivia RH, Coers J.** 2013. IRG and GBP host resistance factors target aberrant, "non-self" vacuoles characterized by the missing of "self" IRGM proteins. PLoS Pathog **9:**e1003414.
42. **Haldar AK, Foltz C, Finethy R, Piro AS, Feeley EM, Pilla-Moffett DM, Komatsu M, Frickel EM, Coers J.** 2015. Ubiquitin systems mark pathogen-containing vacuoles as targets for host defense by guanylate binding proteins. Proc Natl Acad Sci U S A **112:**E5628-5637.
43. **Li P, Jiang W, Yu Q, Liu W, Zhou P, Li J, Xu J, Xu B, Wang F, Shao F.** 2017. Ubiquitination and degradation of GBPs by a Shigella effector to suppress host defence. Nature.
44. **Wandel MP, Pathe C, Werner EI, Ellison CJ, Boyle KB, von der Malsburg A, Rohde J, Randow F.** 2017. GBPs Inhibit Motility of Shigella flexneri but Are Targeted for Degradation by the Bacterial Ubiquitin Ligase IpaH9.8. Cell Host Microbe **22:**507-518 e505.
45. **Man SM, Karki R, Sasai M, Place DE, Kesavardhana S, Temirov J, Frase S, Zhu Q, Malireddi RK, Kuriakose T, Peters JL, Neale G, Brown SA, Yamamoto M, Kanneganti TD.** 2016. IRGB10 Liberates Bacterial Ligands for Sensing by the AIM2 and Caspase-11-NLRP3 Inflammasomes. Cell **167:**382-396 e317.
46. **Bekpen C, Hunn JP, Rohde C, Parvanova I, Guethlein L, Dunn DM, Glowalla E, Leptin M, Howard JC.** 2005. The interferon-inducible p47 (IRG) GTPases in vertebrates: loss of the cell autonomous resistance mechanism in the human lineage. Genome Biol **6:**R92.
47. **Coers J, Starnbach MN, Howard JC.** 2009. Modeling infectious disease in mice: co-adaptation and the role of host-specific IFNgamma responses. PLoS Pathog **5:**e1000333.
48. **Baxt LA, Garza-Mayers AC, Goldberg MB.** 2013. Bacterial subversion of host innate immune pathways. Science **340:**697-701.
49. **Colnot C, Fowlis D, Ripoche MA, Bouchaert I, Poirier F.** 1998. Embryonic implantation in galectin 1/galectin 3 double mutant mice. Dev Dyn **211:**306-313.
50. **Sanjana NE, Shalem O, Zhang F.** 2014. Improved vectors and genome-wide libraries for CRISPR screening. Nat Methods **11:**783-784.
51. **Datsenko KA, Wanner BL.** 2000. One-step inactivation of chromosomal genes in Escherichia coli K-12 using PCR products. Proc Natl Acad Sci U S A **97:**6640-6645.
52. **Cormack BP, Valdivia RH, Falkow S.** 1996. FACS-optimized mutants of the green fluorescent protein (GFP). Gene **173:**33-38.
53. **Eilers B, Mayer-Scholl A, Walker T, Tang C, Weinrauch Y, Zychlinsky A.** 2010. Neutrophil antimicrobial proteins enhance Shigella flexneri adhesion and invasion. Cell Microbiol **12:**1134-1143.
54. **Shen A, Higgins DE.** 2005. The 5' untranslated region-mediated enhancement of intracellular listeriolysin O production is required for Listeria monocytogenes pathogenicity. Mol Microbiol **57:**1460-1473.
55. **Meerbrey KL, Hu G, Kessler JD, Roarty K, Li MZ, Fang JE, Herschkowitz JI, Burrows AE, Ciccia A, Sun T, Schmitt EM, Bernardi RJ, Fu X, Bland CS, Cooper TA, Schiff R, Rosen JM, Westbrook TF, Elledge SJ.** 2011. The pINDUCER lentiviral toolkit for inducible RNA interference in vitro and in vivo. Proc Natl Acad Sci U S A **108:**3665-3670.
56. **Oaks EV, Wingfield ME, Formal SB.** 1985. Plaque formation by virulent Shigella flexneri. Infect Immun **48:**124-129.
57. **Labrec EH, Schneider H, Magnani TJ, Formal SB.** 1964. EPITHELIAL CELL PENETRATION AS AN ESSENTIAL STEP IN THE PATHOGENESIS OF BACILLARY DYSENTERY. J Bacteriol **88:**1503-1518.
58. **Steinhauer J, Agha R, Pham T, Varga AW, Goldberg MB.** 1999. The unipolar Shigella surface protein IcsA is targeted directly to the bacterial old pole: IcsP cleavage of IcsA occurs over the entire bacterial surface. Mol Microbiol **32:**367-377.
59. **Schmitz AM, Morrison, M.F., Agunwamba, A. O., Nibert, M. N. and Lesser, C.F. .** 2009. Protein Interaction Platforms: yeast-based visualization of interacting proteins in living cells. Nature Methods **6:**500-502.

60. **Yi CR, Allen JE, Russo B, Lee SY, Heindl JE, Baxt LA, Herrera BB, Kahoud E, MacBeath G, Goldberg MB.** 2014. Systematic analysis of bacterial effector-postsynaptic density 95/disc large/zonula occludens-1 (PDZ) domain interactions demonstrates Shigella OspE protein promotes protein kinase C activation via PDLIM proteins. J Biol Chem **289:**30101-30113.

61. **Kramer RW, Slagowski NL, Eze NA, Giddings KS, Morrison MF, Siggers KA, Starnbach MN, Lesser CF.** 2007. Yeast functional genomic screens lead to identification of a role for a bacterial effector in innate immunity regulation. PLoS Pathog **3:**e21.

62. **Haraga A, West TE, Brittnacher MJ, Skerrett SJ, Miller SI.** 2008. Burkholderia thailandensis as a model system for the study of the virulence-associated type III secretion system of Burkholderia pseudomallei. Infect Immun **76:**5402-5411.

Figure Legends

Figure 1. Ectopically expressed human GBP1 co-localizes with Gram-negatives *S. flexneri* and *B. thailandensis* but not Gram-positive *L. monocytogenes* in human A549 cells. A549 cells were transfected with indicated GBP paralogs fused to mCherry at their N-termini or transfected with mCherry control. Cells were primed with IFNγ at 200 U/ ml overnight or left untreated. (A) Cells were infected with GFP-positive *S. flexneri* at a multiplicity of infection (MOI) of 50 and microscopy images were taken at 1 hpi. (B) Cells were infected with GFP-positive *B. thailandensis* at an MOI of 100 and images were acquired at 8 hpi. (C) Cells were infected with GFP$^+$ *L. monocytogenes* at an MOI of 5 and monitored at 1 hpi and 3hpi (1 hpi image is shown)**.** (A – B) Combined data from 3 independent experiments are shown. Per experiment >200 bacteria were scored in transfected, *i.e.* mCherry-positive cells. Error bars indicate SEM. Significance was determined by 2-way ANOVA. *** p<0.001; ****p<0.0001; n.s. = non-significant.

Figure 2. Targeting of GBP1 to *S. flexneri* is dependent on its functional G domain, CaaX box and a C-terminal triple-arginine motif. (A) Schematic depiction of critical protein motifs, domains and specific residues within the structure of human GBP1 is shown in**.** (B) A549 or (C – D) HEK 293T cells, respectively, were transfected with the indicated mCherry (control), mCherry-tagged wildtype and variant GBP1/GBP2 expression constructs and infected with GFP$^+$ *S. flexneri* at an MOI of 50 before assessing co-localization at 3 hpi. Combined data from 3 independent experiments are shown. Per experiment >200 bacteria were scored. Error bars indicate SEM. Significance was determined by 1-way ANOVA relative to GBP1 (B) or as indicated (C and D). *p<0.05; *** p<0.001; ****p<0.0001; n.s. = non-significant.

Figure 3. Localization of GBP1 to damaged endosomes is dependent on its triple-arginine motif. 293T cells stably expressing YFP-Galectin-3 (Gal3) were transiently transfected with the indicated expression constructs and approximately 1 day later treated with calcium phosphate precipitates to induce endosomal damage leading to YFP-Gal3 puncta formation. (A and B) Combined data from 3 independent experiments are shown. Per independent experiment >400 YFP-Gal3 puncta were scored for GBP1 co-localization in mCherry-positive cells. Error bars denote SEM. 1-way ANOVA was used to assess significance. **p<0.01; *** p<0.001; ****p<0.0001; n.s. = non-significant. (B) Arrows within representative images point to Galectin-3-positive vacuoles.

Figure 4. Bacterial targeting of GBP1 is diminished for *S. flexneri* rough mutants. (A) Arrows indicate site of truncation to LPS structure resulting from the loss-of-function mutations in bacterial genes *galU* and *rfa.* (B) 293T cells were transfected with mCherry-GBP1 or mCherry control, whereas (C) HeLa cells were left untransfected. Following infection with wildtype or the indicated *S. flexneri* mutants at an MOI of 50, co-localization of (B) ectopically expressed GBP1 or (C) endogenous GBP1 was quantified. Combined data from at least 3 independent experiments are shown. Per experiment >400 bacteria were scored per experiemental condition. Error bars represent SEM. 2-way ANOVA was used to assess statistical significance. *** p<0.001; ****p<0.0001; n.s. = non-significant.

Figure 5. GBP1-tagged *S. flexneri* replicate within intracellular bacterial aggregates. (A) IFNγ-primed and unprimed HeLa were infected at an MOI of 50 with *S. flexneri* carrying an IPTG-inducible GFP reporter plasmid. IPTG, and where indicated also chloramphenicol (Cm), were added to the culture medium at 2 hpi. At 4 hpi cells were fixed and stained with anti-LPS (blue) and

anti-GBP1 (red). A representative image of infected, IFNγ-primed HeLa cells is shown. (B) Combined data from 3 independent experiments as described under (A) are shown. (C) Protein lysates from IFNγ-primed parental HeLa (WT) and two independent *GBP1^{KO}* clones were transferred to membranes and probed with anti-GBP1 and anti-GAPDH antibodies. (D) Two independent *GBP1^{KO}* HeLa cell clones were transfected with wildtype GBP1 or GBP1$^{R584\text{-}586A}$ mCherry fusion proteins and then infected with *S. flexneri* at an MOI of 50. Bacteria were visualized via with anti-LPS (blue) immunostaining. Cluster analysis was performed as described in Materials and Methods. (E) *GBP1^{KO}* HeLa cells were transfected with mCherry-GBP1 and infected with poly-D-Lysine pre-treated *S. flexneri* at an MOI of 10. Cells were infected for 30 minutes, washed and then placed in Phenol-red free DMEM. Video microscopy was begun at 2 hpi (2:00). Images of 6-minute intervals between 2:00 and 2:42 are shown. Arrowheads point at bacteria that have undergone cell division. 2-way ANOVA was used to assess statistical significance. ****p<0.0001; n.s. = non-significant.

Figure 6. GBP1 restricts actin tail formation and cell-to-cell spread via its triple-arginine motif. (A) 293T cells were transfected with mCh-GBP1 and then infected with wildtype (WT) or *⊿icsA S. flexneri* at an MOI of 50. Confocal images were taken at 3 hpi and analysed for actin tail formation as described under Materials and Methods. Data are combined from 3 independent experiments. Per experiment and condition >550 bacteria were examined in mCherry-positive cells. (B) Parental HeLa-Cas9 (WT) and *GBP1^{KO}* cells were transfected with mCherry-GBP1 or mCherry-GBP1$^{R584\text{-}586A}$ as indicated, then primed with IFNγ overnight and infected with *S. flexneri* at an MOI of 50. Cells were fixed and stained at 3 hpi and representative images are shown. Bacterial actin tail formation inside mCherry-positive cells was quantified and combined data from 3 independent data are shown. (C) Plaque assays on IFNγ-primed cells were performed as

described under Materials and Methods and combined data from 3 independent experiments as well as representative images are shown. (D) HeLa-Cas9 (WT) cells or *GBP1*^{KO} (clone #1) with stably integrated pInducer-GBP1 or pInducer-GBP1$^{R584\text{-}586A}$ expression constructs where either primed with IFNγ or stimulated with 1 µg/ml of aTc, as indicated. Combined data from 3 independent experiments are shown. Error bars depict SEM (A – C) or standard deviation (D). 2-way (A – B) or 1-way ANOVA (C – D) were used to determine statistical significance. **p<0.01; ***p<0.001; ****p<0.0001; n.s. = non-significant.

Figure 7. Endogenous GBP1 co-localizes with *S. flexneri* and recruits additional GBP paralogs in HeLa but not in A549 cells. (A) HeLa-Cas9 (WT) and *GBP1*^{KO} cells were transfected with indicated mCherry-GBP expression constructs and primed with IFNγ overnight. Cells were infected with GFP^{+} *S. flexneri* at an MOI of 50, fixed at 3 hpi and mCherry-positive cells were analysed for bacterial co-localization with GBPs. The combined data from 3 independent experiments are shown. Per experiment and condition >300 bacteria were scored. Error bars denote SEM and student t-tests were used to determine statistical significance. (B) IFNγ-primed HeLa and A549 cells were infected with GFP^{+} *S. flexneri* at an MOI of 50 or GFP^{+} *B. thailandensis* at an MOI of 100 and fixed and stained with anti-GBP1 at 3 hpi or 8 hpi, respectively. Combined data are from 3 independent experiments (>600 bacteria counted per experiment) are shown. Error bars represent SEM and 2-way ANOVA was used to assess significance. (C) Expression of endogenous GBP1 in IFNγ-primed HeLa and A549 cells was assessed by Western blotting. (D) *GBP1*^{KO} HeLa cells with stably integrated pInducer-GBP1 were stimulated overnight with indicated concentrations of aTc and protein lysates were subjected to Western blotting. Protein lysates from IFNγ-primed A549 and HeLa-Cas9 were included for comparison. (E) *GBP1*^{KO} HeLa cells with stably integrated pInducer-GBP1 were stimulated overnight with indicated concentrations of aTc,

then infected with GFP$^+$ *S. flexneri* (MOI of 50) for 3 h or GFP$^+$ *B. thailandensis* (MOI 100) for 8 h and analyzed for bacterial co-localization with endogenous GBP1. Combined data from 3 independent experiments (>400 bacteria counted per experiment) are shown. Error bars represent SEM. *p<0.05; **p<0.01; ***p<0.001; n.s. = non-significant.

Figure 8. IpaH9.8 blocks GBP1 recruitment and GBP1-mediated inhibition of actin-based motility. (A) IFNγ-primed HeLa and A549 cells were infected with the indicated *S. flexneri* strains at an MOI of 50 and at 3 hpi processed and analyzed for co-localization with endogenous GBP1. Data are combined from 3 independent experiments scoring 600 bacteria per experiment. 1-way ANOVA was used to determine significance. (B) Experiments were conducted as in (A) with the *S. flexneri* mutant strains, as listed. 2-way ANOVA was used to determine significance of combined data from 3 independent experiments. (C) IFNγ-primed HeLa-Cas9 and derived *GBP1^{KO}* cells were infected with the indicated *S. flexneri* mutant strains. Representative images of plaques are shown. Combined data from 3 independent experiments are depicted. Error bars indicate SD. 2-way ANOVA was used to determine significance. **p<0.01; ***p<0.001; ****p<0.0001; n.s. = non-significant.

Supplementary text

Supplementary Figure Legends

Figure S1. Expression of N-terminal mCherry-GBP fusion proteins in 293T cells. 293T cells were transiently transfected with mCherry-tagged human GBPs. Cells were lysed in RIPA buffer approximately 24 h post transfection and probed with anti-GBP1 and anti-GAPDH antibodies.

Figure S2. GBP1 co-localizes with *S. flexneri* independent of Galectin-3. Primary WT (C57BL/6J) and *Galectin-3*$^{-/-}$ MEFs were transiently transfected with expression constructs for mCh-GBP1 or an mCherry control, and subsequently infected with GFP^{+} *S. flexneri* at an MOI of 50. Cells were fixed at 3 hpi, and the percentage of GBP1-positive bacteria was determined by microscopy. Graph represents the mean percentage of GBP1-positive bacteria from three independent experiments. Error bars denote SEM. A 2-way ANOVA was used for statistical analysis. n.s. = non-significant.

Supplementary Videos

Video S1. *GBP1*^{KO} HeLa cells transfected with mCherry-GBP1 were infected with poly-D-lysine pre-treated *S.flexneri* expressing GFP at an MOI of 10. Images were collected every 30 seconds for 3 hours, beginning at 10 minutes post infection.

Video S2. *GBP1*^{KO} HeLa cells transfected with mCherry-GBP1 were infected with poly-D-lysine pre-treated *S.flexneri* expressing GFP at an MOI of 10. Images were collected every 90 seconds for 45 minutes, beginning at 190 minutes post infection.

Tables

Mutation	Notes	Protein Size
deletion 668-729	Deletion resulting in frame shift and early stop codon	234 aa
deletion 667-730	Deletion resulting in frame shift and early stop codon	245 aa

Table S1. *GBP1* alleles in HeLa *GBP1*^{KO} clones #1 and #2. Deletion is annotated based on the corresponding nucleotide positions in GBP1 ORF. The predicted protein size of truncated protein resulting from the mutation is provided (full-length GBP1 is 592 amino acids in length).

Species	Strain	Characteristics	Reference
S.flexneri	WT	2457T	(57)
S.flexneri	*ΔicsA*	2457T *ΔicsA*	(58)
S.flexneri	*galU*	2457T with mutant *galU*	(30)
S.flexneri	*rfaL*	2457T with mutant *rfaL*	(30)
S.flexneri	*ΔmxiE*	2457T *ΔmxiE*	This work
S.flexneri	*Δspa15*	2457T *Δspa15*	(59)
S.flexneri	*ΔospB*	2457T *ΔospB*	This work
S.flexneri	*ΔospC1*	2457T *ΔospC1*	This work
S.flexneri	*ΔospE1/2*	2457T *ΔospE1/2*	(60)
S.flexneri	*ΔospF*	2457T *ΔospF*	(61)
S.flexneri	*ΔvirA*	2457T *ΔvirA*	This work
S.flexneri	*ΔipaH1.4*	2457T *ΔipaH1.4*	This work
S.flexneri	*ΔipaH4.5*	2457T *ΔipaH4.5*	This work
S.flexneri	*ΔipaH7.8*	2457T *ΔipaH7.8*	This work
S.flexneri	*ΔipaH9.8*	2457T *ΔipaH9.8*	This work
B.thailandensis	WT	American Type Culture Collection 700388 expressing GFP	(62)
L.monocytogenes	WT	10403S expressing GFP	(54)

Table S2. List of bacterial strains used in this study

Oligomers	**Sequence** (5' to 3')
MxiE-5'	CTATCATGAGAATGATCTTCGGGATAGTTGAATACCGAAGTGTAGGCTGGAGCTGCTTC
MxiE-3'	CTAACCGCCAAGTGTTCAGTTGTTCTTTGACTTTTGCCCCCATATGAATATCCTCCTTAG
OspB-5'	TTTATAAAACAATATATGGAGTCATGTAGGTATGAATTTAGTGTAGGCTGGAGCTGCTTC
OspB-3'	CCCTCCATAGCCTGATACAGGCTGTCCAGCTTTATGGGGTCATATGAATATCCTCCTTAG
OspC1-5'	ATTAAAACTGTTTTCATATAAGGTTCATTTTATGAATATAGTGTAGGCTGGAGCTGCTTC
OspC1-3'	CTGCCTTTTGCTAAACGATATTCAATTTTGATTAAATATACATATGAATATCCTCCTTAG
VirA-5'	ATTAATAGGAAAATACATCAGGAGAAATCAAATGCAGACAGTGTAGGCTGGAGCTGCTTC
VirA-3'	TTTACAGTCTGGCAGCCAATATAATATTGGCTTAAACATCCATATGAATATCCTCCTTAG
IpaH1.4-5'	ATCTGGTTAACCCATATACAAGGGAGACAGAATGACCGAAGTGTAGGCTGGAGCTGCTTC
IpaH1.4-3'	GGGGGGTGCCCCTATTAAGTTGTCAAGCATGTTATGACCCCATATGAATATCCTCCTTAG
IpaH4.5-5'	GACCAAGATATGAATAGTGAGGGGTTAATAAATGAAACCGGTGTAGGCTGGAGCTGCTTC
IpaH4.5-3'	GAAGTTTAGTCTCCAGGATTCCCGGGGCGGTTCAGGCCAGCATATGAATATCCTCCTTAG
IpaH7.8-5'	ATTCTCACAAATATAAGGTGGACCTAGCATTATGTTCTCTGTGTAGGCTGGAGCTGCTTC
IpaH7.8-3'	CCGGTCTGCGGTTTATGCTTATGCGACGTGATTATGAATGCATATGAATATCCTCCTTAG
IpaH9.8-5'	AACTCCTACTTATTTCTTTTAACAAAGCCATTTGTCCACCGTGTAGGCTGGAGCTGCTTC
IpaH9.8-3'	TCACTGGCGCTGACAGTTTTATGCGATGTGATTATGAATGCATATGAATATCCTCCTTAG

Table S3. List of DNA oligomers used to generate *S. flexneri* mutant strains

Oligomer	**Sequence** (5' to 3')	**Restriction Site**
GBP1-F	AAGAACTAGATCTATGGCATCAGAGATCCACATGACAG	Bgl II
GBP1-R	CGGCCGCCCGGGTTAGCTTATGGTACATGCCTTTCGTCG	XmaI
GBP2-F	AAGAACTAGATCTATGGCTCCAGAGATCAACTTGCC	Bgl II
GBP2-R	CGGCCGCCCGGGTTAGAGTATGTTACATATTGGCTCCAATGATTTGC	XmaI
GBP3-F	CTGGAACTCGAGGGATGGCTCCAGAGATCCACATGAC	XhoI
GBP3-R	CGGCCGCCCGGGTTAGATCTTTAGCTTATGCGACATATATCTCTTGG	XmaI
GBP4-F	AAGAACTAGATCTATGGGTGAGAGAACTCTTCACGC	Bgl II
GBP4-R	CGGCCGCCCGGGTTAAATACGTGAGCCAAGATATTTTGTCCCT	XmaI
GBP5-F	CTGGAACTCGAGGGATGGCTTTAGAGATCCACATGTCAGA	XhoI
GBP5-R	CGGCCGCCCGGGTTAGAGTAAAACACATGGATCATCGTTATTAACAG	XmaI
GBP6-F	AAGAACTAGATCTATGGAATCTGGACCCAAAATGTTGG	Bgl II
GBP6-R	CGGCCGCCCGGGTTAAAAGGGGAGCTTATGCTTTTTAAAGAGTG	XmaI
GBP7-F	AAGAACTAGATCTATGGCATCAGAGATCCACATGC	Bgl II
GBP7-R	CGGCCGCCCGGGTCAGCTTATAATTTTCTTACCAGGATTTCTCAGC	XmaI

Table S4 List of oligomers and restriction sites used to generate mCherry GBP fusion expression constructs

Oligomer	**Sequence** (5' to 3')
GBP1-BclI-F	GACTGATGCAATTCTCCAGACTGATCAGACTCTCACAGAA
GBP1-BclI-R	TTCTGTGAGAGTCTGATCAGTCTGGAGAATTGCATCAGTC
GBP1^{R48A}-F	GCAATTGTGGGCCTCTACGCCACAGGCAAATCCTACCTGATG
GBP1^{R48A}-R	CATCAGGTAGGATTTGCCTGTGGCGTAGAGGCCCACAATTGC
GBP1^{K51A}-F	ATTGTGGGCCTCTACCGCACAGGCGCATCCTACCTGATGAACAAG
GBP1^{K51A}-R	CTTGTTCATCAGGTAGGATGCGCCTGTGCGGTAGAGGCCCACAAT
GBP1^{S52N}-F	CTCTACCGCACAGGCAAAAACTACCTGATGAACAAGCTGGCT
GBP1^{S52N}-R	AGCCAGCTTGTTCATCAGGTAGTTTTTGCCTGTGCGGTAGAG
GBP1$^{\Delta 589-592}$-F	GAAAATGAGACGACGAAAGGCATAACCCGGGATCCA
GBP1$^{\Delta 589-592}$-R	TGGATCCCGGGTTATGCCTTTCGTCGTCTCATTTTC
GBP1^{C589A}-F	AGACGACGAAAGGCAGCCACCATAAGCTAACCCGGGAT
GBP1^{C589A}-R	ATCCCGGGTTAGCTTATGGTGGCTGCCTTTCGTCGTCT
GBP1/2^{CaaX}-F	CGAAAGGCATGTAACATACTCTAACCCGGGATCCACCGG
GBP1/2^{CaaX}-R	CCGGTGGATCCCGGGTTAGAGTATGTTACATGCCTTTCG
GBP2/1^{CaaX}-F	GAGCCAATATGTACCATAAGCTAACCCGGGATCCACCGG
GBP2/1^{CaaX}-R	CCGGTGGATCCCGGGTTAGCTTATGGTACATATTGGCTC
GBP1$^{\Delta PBM}$-F	GATCTCCAGACGAAAGCATGTACCATAAGC
GBP1$^{\Delta PBM}$-R	GCTTATGGTACATGCTTTCGTCTGGAGATC
GBP1$^{R584-586A}$-F	GAGATACAGGATCTCCAGACGAAAATGGCAGCAGCAAAGGCATGTACCATAAGCTAAC
GBP1$^{R584-586A}$-R	GTTAGCTTATGGTACATGCCTTTGCTGCTGCCATTTTCGTCTGGAGATCCTGTATCTC
GBP2^{+PBM}-F	GAGAAGCAAATCATTGGAGCCAAAAATGAGACGACGAAAGATATGTAACATACTC
GBP2^{+PBM}-R	GAGTATGTTACATATCTTTCGTCGTCTCATTTTTGGCTCCAATGATTTGCTTCTC
GBP2^{I587A}-F	AGAAGCAAATCATTGGAGCCAGCATGTAACATACTCTAACCC
GBP2^{I587A}-R	GGGTTAGAGTATGTTACATGCTGGCTCCAATGATTTGCTTCT
GBP1-attB1-F	GGGGACAAGTTTGTACAAAAAAGCAGGCTGCCACCATGGCATCAGAGATCCACATGACAG
GBP1-attB2-R	GGGGACCACTTTGTACAAGAAAGCTGGGTCTTAGCTTATGGTACATGCCTTTCGTC

Table S5. Oligomers used to generate GBP mutant and chimeric variants.

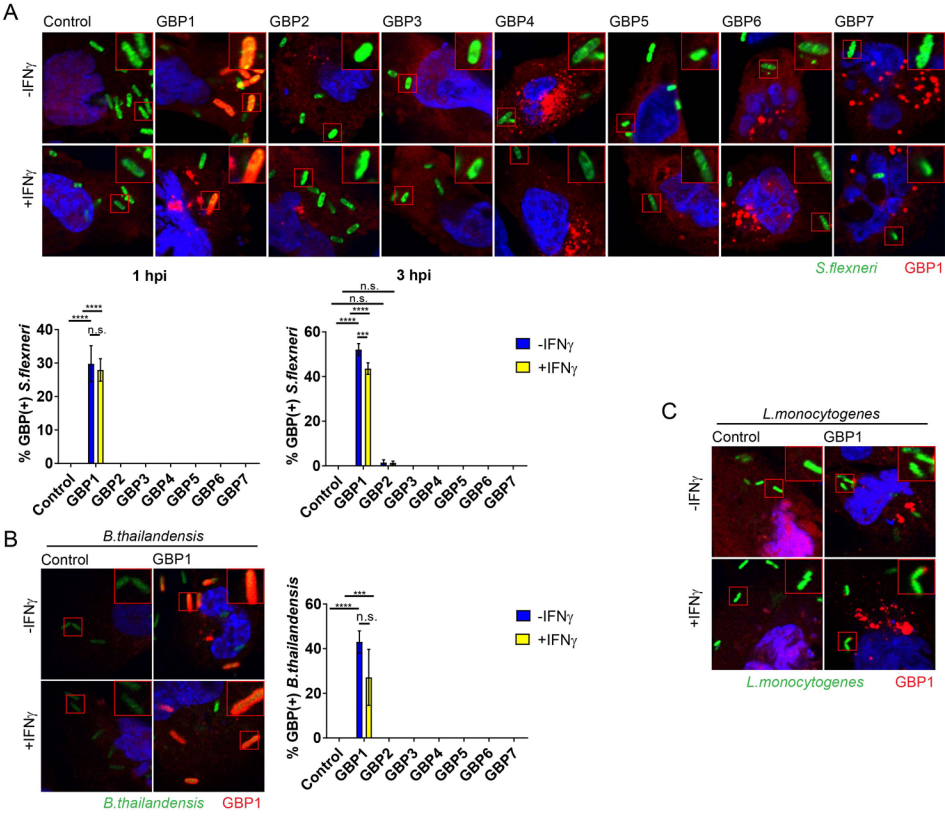
A
Control
GBP1
GBP2
GBP3
GBP4
GBP5
GBP6
GBP7
-IFNγ
+IFNγ
S.flexneri
GBP1
1 hpi
3 hpi
% GBP(+) S.flexneri
n.s.
****
***
-IFNγ
+IFNγ
B
B.thailandensis
Control
GBP1
-IFNγ
+IFNγ
B.thailandensis
GBP1
% GBP(+) B.thailandensis
C
L.monocytogenes
Control
GBP1
-IFNγ
+IFNγ
L.monocytogenes
GBP1

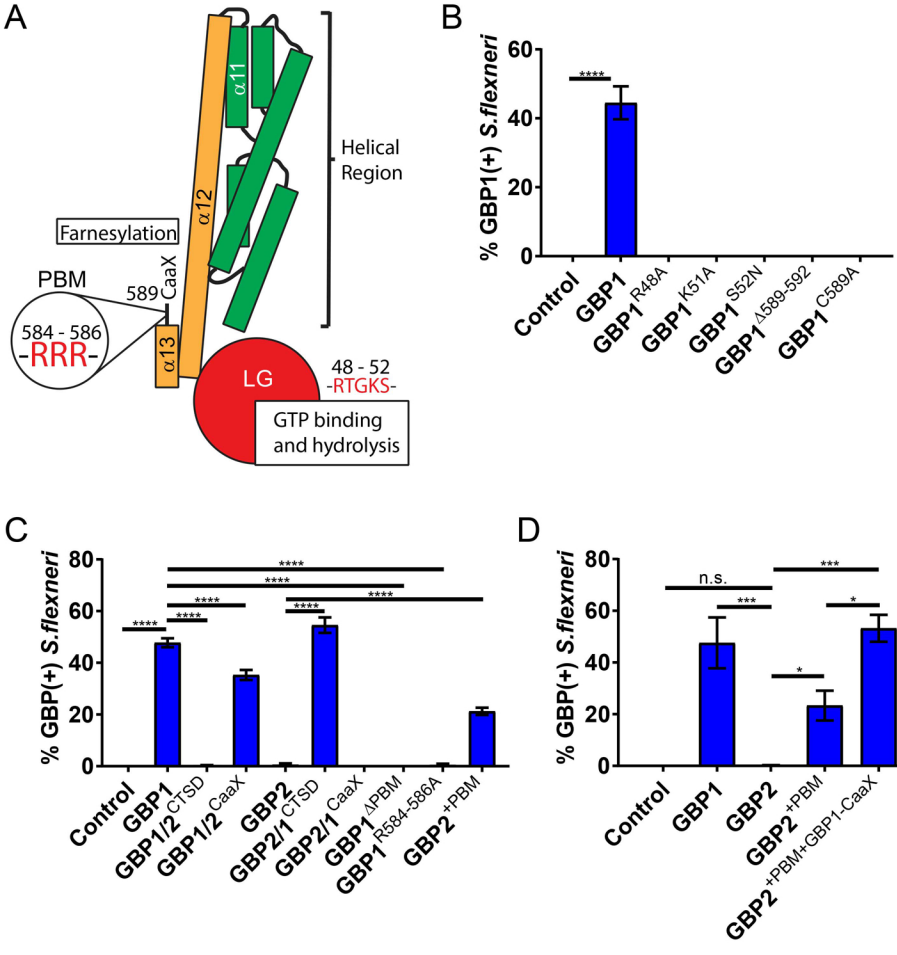
A
α11
α12
α13
Helical Region
Farnesylation
PBM
589 CaaX
584 - 586
-RRR-
LG
48 - 52
-RTGKS-
GTP binding and hydrolysis
B
% GBP1(+) S.flexneri
60
40
20
0
****
Control
GBP1
GBP1R48A
GBP1K51A
GBP1S52N
GBP1Δ589-592
GBP1C589A
C
% GBP(+) S.flexneri
80
60
40
20
0
****
Control
GBP1
GBP1/2CTSD
GBP1/2CaaX
GBP2
GBP2/1CTSD
GBP2/1CaaX
GBP1ΔPBM
GBP1R584-586A
GBP2+PBM
D
% GBP(+) S.flexneri
80
60
40
20
0
n.s.
***
*
Control
GBP1
GBP2
GBP2+PBM
GBP2+PBM+GBP1-CaaX

A

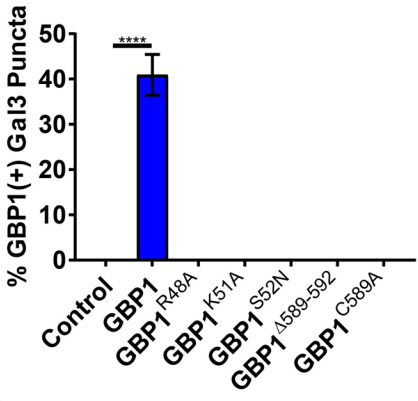
% GBP1(+) Gal3 Puncta
50
40
30
20
10
0
****
Control
GBP1
GBP1R48A
GBP1K51A
GBP1S52N
GBP1Δ589-592
GBP1C589A

B

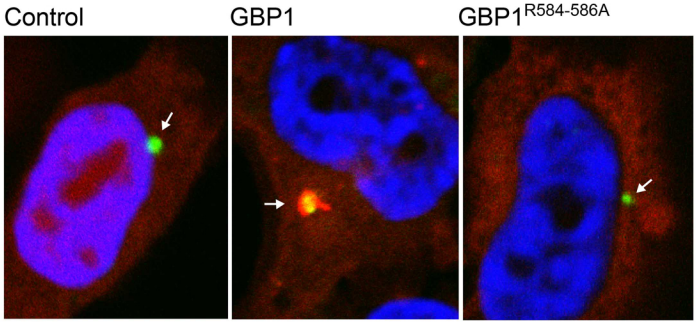
Control
GBP1
GBP1R584-586A
Galectin-3
GBP1

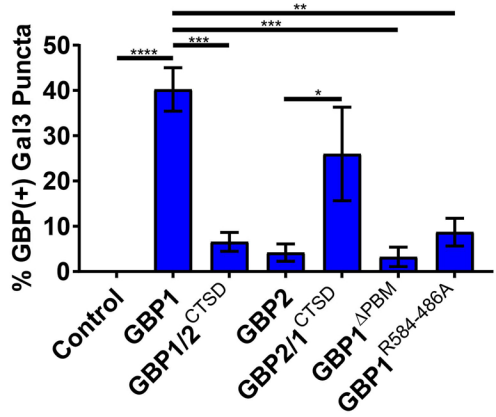
% GBP(+) Gal3 Puncta
50
40
30
20
10
0
**
***
***
****
*
Control
GBP1
GBP1/2CTSD
GBP2
GBP2/1CTSD
GBP1ΔPBM
GBP1R584-486A

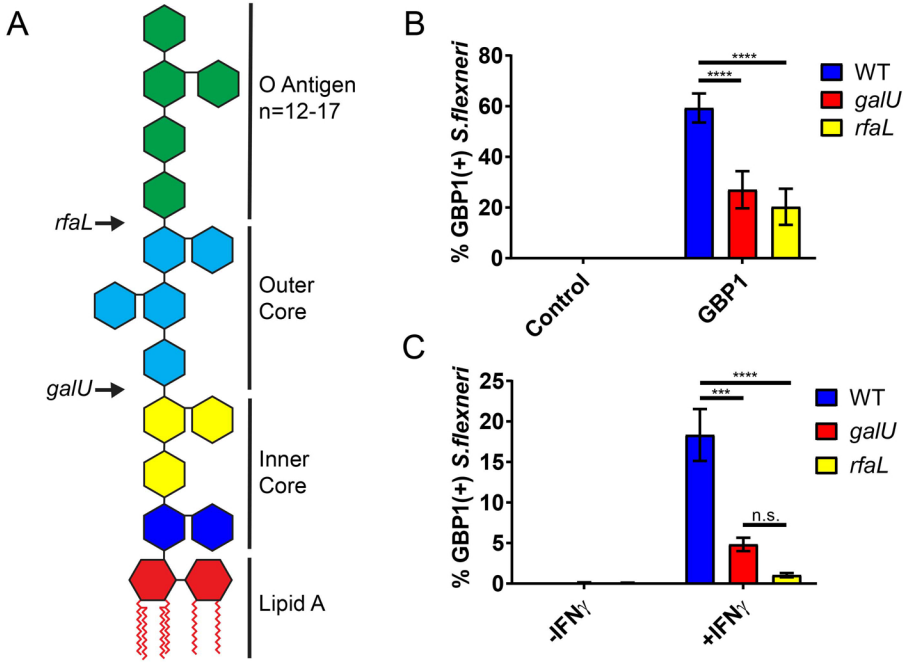
A
O Antigen
n=12-17
rfaL
Outer
Core
galU
Inner
Core
Lipid A
B
% GBP1(+) S.flexneri
80
60
40
20
0
****
****
WT
galU
rfaL
Control
GBP1
C
% GBP1(+) S.flexneri
25
20
15
10
5
0
****
***
n.s.
WT
galU
rfaL
-IFNγ
+IFNγ

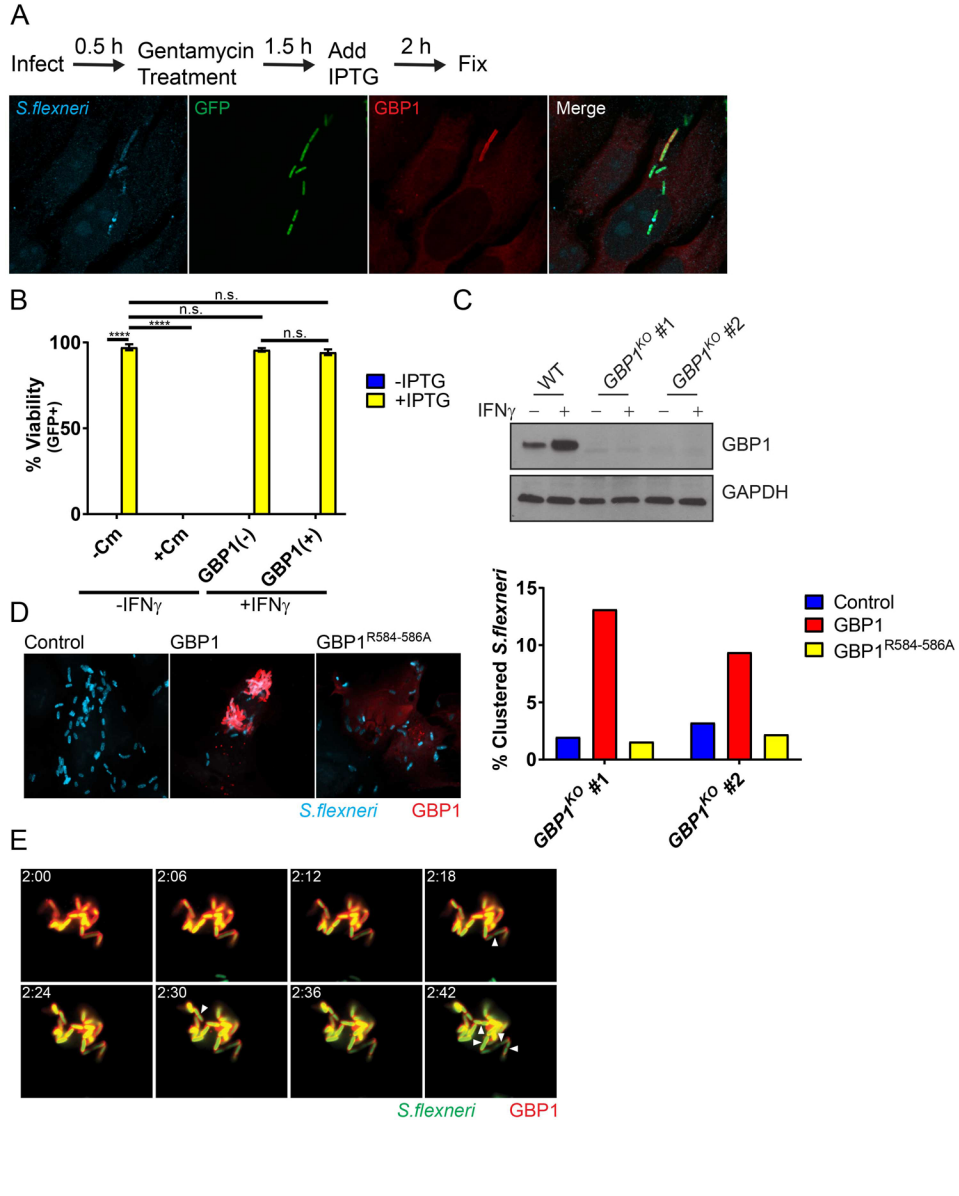
A
Infect
0.5 h
Gentamycin Treatment
1.5 h
Add IPTG
2 h
Fix
S.flexneri
GFP
GBP1
Merge
B
n.s.
n.s.
****
****
n.s.
100
50
0
% Viability (GFP+)
-IPTG
+IPTG
-Cm
+Cm
GBP1(-)
GBP1(+)
-IFNγ
+IFNγ
C
WT
GBP1KO #1
GBP1KO #2
IFNγ – + – + – +
GBP1
GAPDH
D
Control
GBP1
GBP1R584-586A
S.flexneri
GBP1
% Clustered S.flexneri
15
10
5
0
Control
GBP1
GBP1R584-586A
GBP1KO #1
GBP1KO #2
E
2:00
2:06
2:12
2:18
2:24
2:30
2:36
2:42
S.flexneri
GBP1

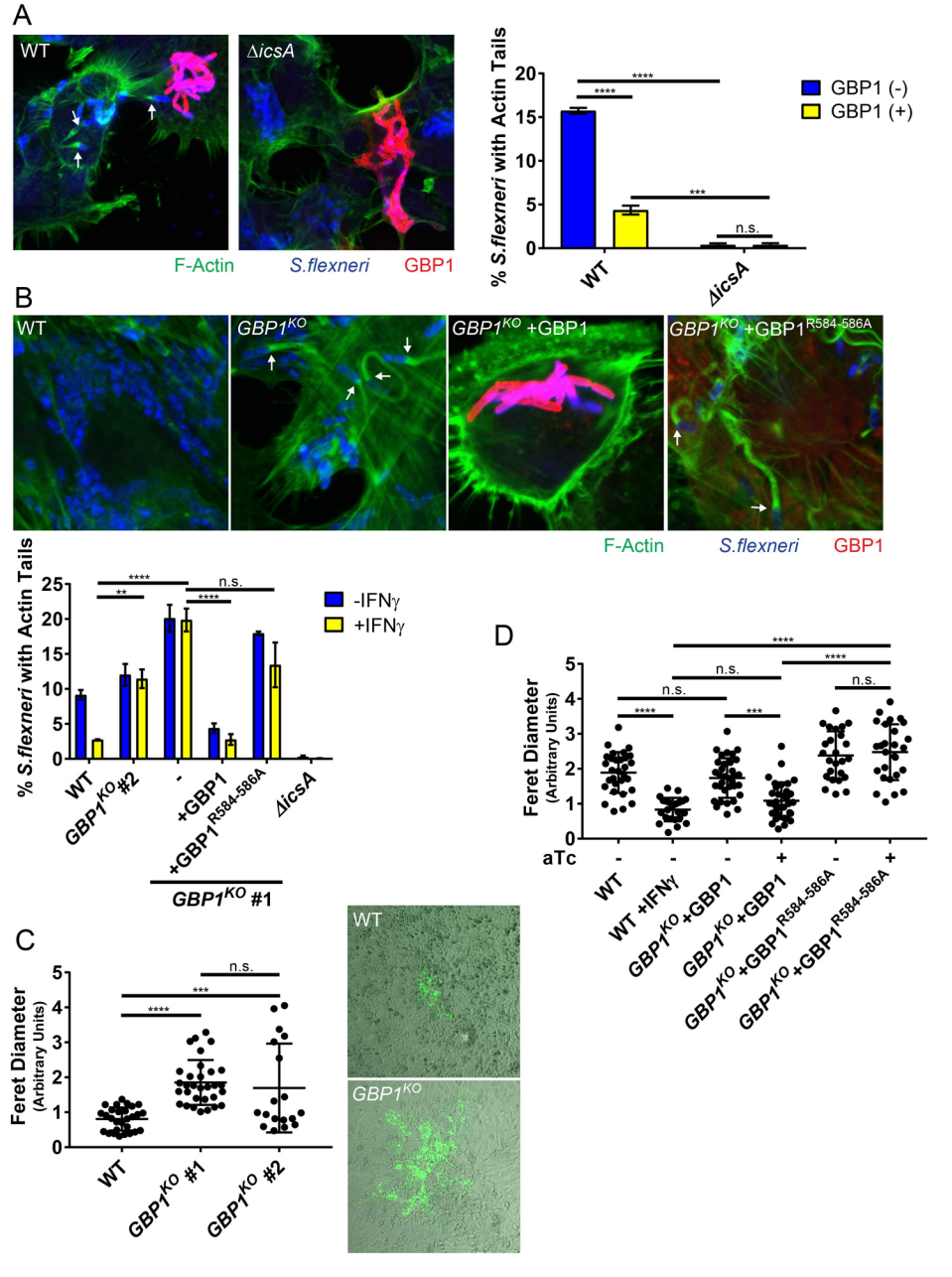
A
WT
ΔicsA
F-Actin
S.flexneri
GBP1
% S.flexneri with Actin Tails
GBP1 (-)
GBP1 (+)
****
****
***
n.s.
WT
ΔicsA
B
WT
GBP1KO
GBP1KO +GBP1
GBP1KO +GBP1R584-586A
F-Actin
S.flexneri
GBP1
% S.flexneri with Actin Tails
-IFNγ
+IFNγ
WT
GBP1KO #2
+GBP1
+GBP1R584-586A
ΔicsA
GBP1KO #1
C
Feret Diameter (Arbitrary Units)
WT
GBP1KO #1
GBP1KO #2
WT
GBP1KO
D
Feret Diameter (Arbitrary Units)
aTc
WT
WT +IFNγ
GBP1KO +GBP1
GBP1KO +GBP1
GBP1KO +GBP1R584-586A
GBP1KO +GBP1R584-586A

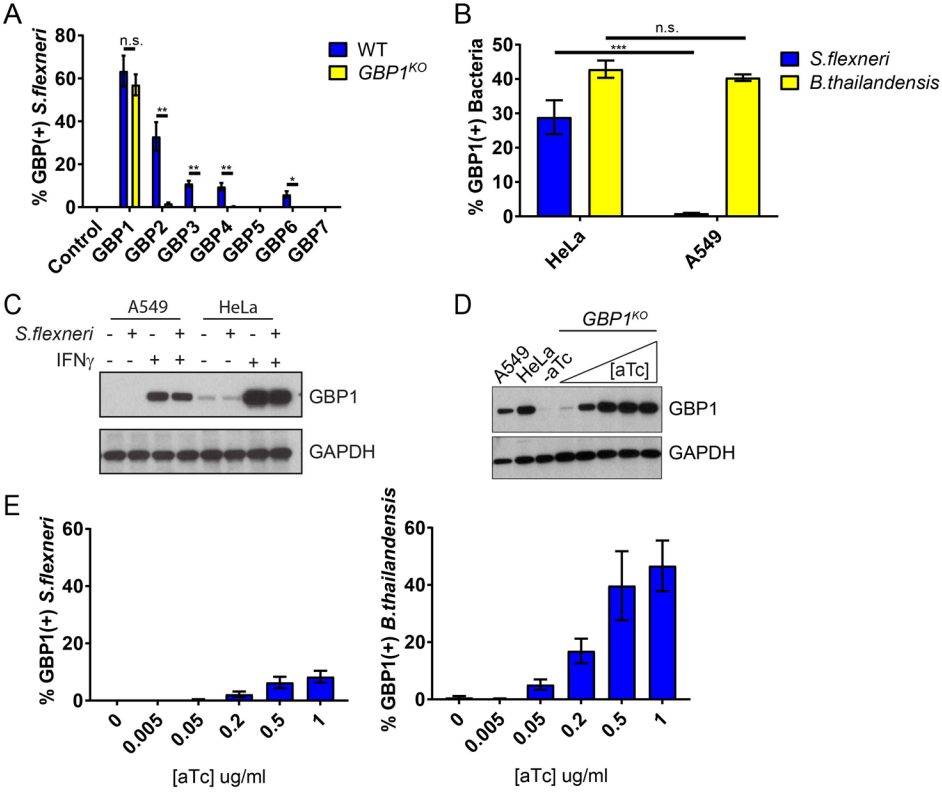
A
% GBP(+) S.flexneri
n.s.
WT
GBP1KO
Control
GBP1
GBP2
GBP3
GBP4
GBP5
GBP6
GBP7
B
% GBP1(+) Bacteria
n.s.
***
S.flexneri
B.thailandensis
HeLa
A549
C
A549
HeLa
S.flexneri
IFNγ
GBP1
GAPDH
D
GBP1KO
A549
HeLa
-aTc
[aTc]
GBP1
GAPDH
E
% GBP1(+) S.flexneri
% GBP1(+) B.thailandensis
0
0.005
0.05
0.2
0.5
1
[aTc] ug/ml

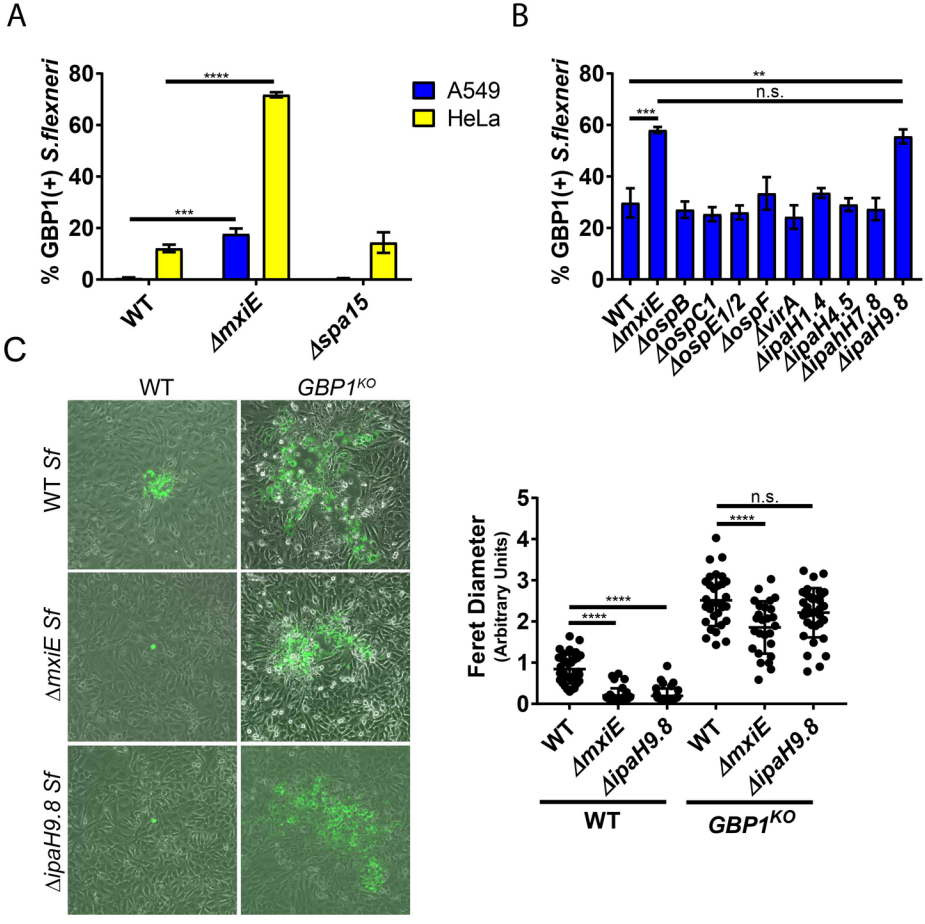
A
% GBP1(+) S.flexneri
80
60
40
20
0
****
***
A549
HeLa
WT
ΔmxiE
Δspa15
B
% GBP1(+) S.flexneri
**
n.s.
***
WT
ΔmxiE
ΔospB
ΔospC1
ΔospE1/2
ΔospF
ΔvirA
ΔipaH1.4
ΔipaH4.5
ΔipaH7.8
ΔipaH9.8
C
WT
GBP1KO
WT Sf
ΔmxiE Sf
ΔipaH9.8 Sf
Feret Diameter
(Arbitrary Units)
5
4
3
2
1
0
n.s.
****
****
****
WT
ΔmxiE
ΔipaH9.8
WT
ΔmxiE
ΔipaH9.8
WT
GBP1KO

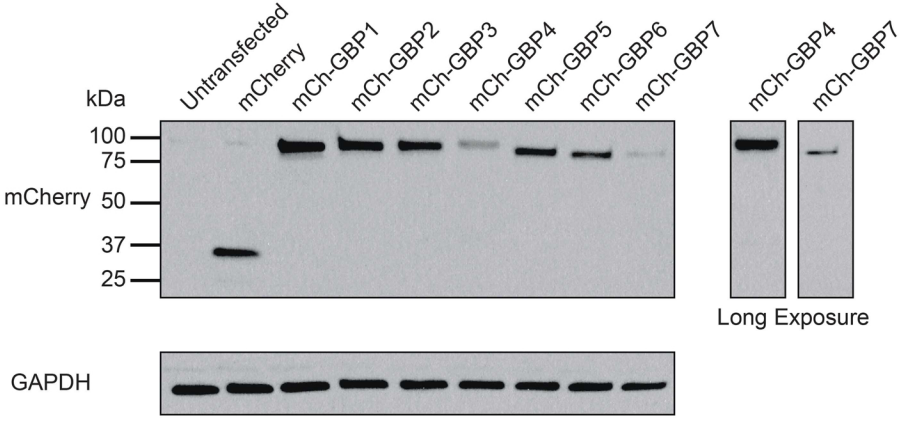
Untransfected
mCherry
mCh-GBP1
mCh-GBP2
mCh-GBP3
mCh-GBP4
mCh-GBP5
mCh-GBP6
mCh-GBP7
mCh-GBP4
mCh-GBP7
kDa
100
75
mCherry
50
37
25
Long Exposure
GAPDH

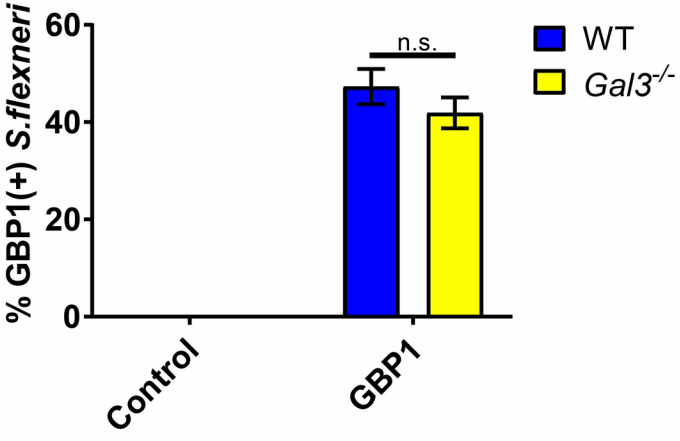
% GBP1(+) S.flexneri
60
40
20
0
n.s.
WT
Gal3-/-
Control
GBP1